Acoustic Scattering from Fluid Bodies of Arbitrary Shape

B. Chandrasekhar[1] and Sadasiva M. Rao[2]

Abstract: In this work, a simple and robust numerical method to calculate the scattered acoustic fields from fluid bodies of arbitrary shape subjected to a plane wave incidence is presented. Three formulations are investigated in this work *viz*. the single layer formulation (SLF), the double layer formulation (DLF), and the combined layer formulation (CLF). Although the SLF and the DLF are prone to non-uniqueness at certain discrete frequencies of the incident wave, the CLF is problem-free, eliminates numerical artifacts, and provides a unique solution at all frequencies. Further, all the three formulations are surface formulations which implies that only the scatterer surface is discretized for the numerical solution. The numerical solution is obtained by approximating the fluid body surface by triangular patches and adopting the method of moments (MoM) solution procedure. Finally, several numerical examples have been presented to highlight the capabilities of the present work.

Keyword: acoustic scattering, fluid bodies, arbitrary shape

1 Introduction

The accurate calculation of scattered/penetrated acoustic fields by a fluid body immersed in an infinite, homogeneous, non-viscous medium, such as a fish in a large pond, has commercial/defense applications in many different areas such as medical electronics, marine navigation, sonar, and so on. The solution to these type of problems is usually obtained using numerical methods since the object shape can be arbitrary. Fortunately, the numerical methods, although approximate, can yield highly accurate results mainly due to the recent advances in the computer industry.

In so far as the numerical methods are concerned, the most popular techniques deal with either differential equation (DE) solution methods or integral equation (IE) solution methods. Note that, for the type of problems discussed in this work, IE solution methods are more efficient than DE methods, simply because in case of IE methods one needs to describe only the body surface to the computer whereas for a DE solution the volume, both outside as well as inside, need to be descretized.

For the IE solution methods, the most popular numerical technique is the so-called boundary integral equation (BIE) method [Tobocman(1984a), Tobocman(1984b), and Seybert and Casey (1988)] based on the application of Helmholtz integral equation to fluid body scattering problems. Also, the same problem was solved [Rao, Raju, and Sun (1992)] via potential theory [Kellog (1929)] and the method of moments (MoM) [Harrington (1968)]. Previously, alternate integral equations, viz. PFIE, VFIE and CFIE, were developed [Sun (1991) and Rao, Raju, and Sun (1991)] to tackle resonance problem associated with fluid body scattering. However, they presented only 2D case and it's extension to 3D case need to be investigated. Although these methods are quite general and applicable to arbitrary bodies, the methods fail at certain discrete frequencies referred to as it characteristic frequencies. Note that the characteristic frequencies are simply the resonance frequencies of a same shaped cavity as that of the scatterer. Further, when the frequency of the incident field is in the vicinity of any one frequency of the characteristic frequency set, then the solution tends to he highly erroneous. In fact, this problem is quite severe at higher frequencies since

[1] Super Computer Education Research Centre, Indian Institute of Science, Bangalore, India.
[2] Department of Electrical and Computer Engineering, Auburn University, Auburn, U.S.A

the discrete characteristic frequencies are densely packed in this range and there is no way of assessing the accuracy of the solution. More details regarding the fictitious frequencies can be found in [Chen, Chen, and Chen (2006) and Chen (2006)]. A remedy proposed for this problem is to apply the CHIEF method [Schenck (1968) and Benthien and Schenck (1997)]. In fact, the CHIEF method was applied only to rigid bodies and extremely cumbersome for fluid bodies. Leis [Leis (1965)], Panich [Panich (1965)], Brakhage and Werner [Brakhage and Werner (1965)] and Burton and Miller [Burton and Miller (1971)] demonstrated that by combining the single layer and double layer potentials with a complex coupling parameter, the non-uniqueness problem can be averted. Many researchers [Amini andWilton (1986),Meyer, Bell, Zinn, and Stallybras (1978), Chien, Raliyah and Alturi (1990), Yan, Cui and Hung (2005)] attempted to implement the BM procedure to overcome the internal resonance problem. The usual procedure is to regularize the hypersingular integral and the regularization technique is computationally very expensive and it is difficult to incorporate in a general-purpose code. Also, there are other methods which reduce the hyper singular kernel to a strongly singular kernel and their solution is based on based on Petrov-Galerkin schemes [Qian, Han, and Atluri (2004)] and collocation-based boundary element method [Qian, Han, Ufimtsev, and Atluri (2004)]. A de-singularized boundary integral formulation is also one of the recently proposed method [Callsen, von Estorff, and Zaleski (2004)] to overcome the problems of singularity. Recently, an alternate method was presented in [Chandrasekhar and Rao (2004)] to overcome the non-uniqueness problem based on the work of Burton and Miller [Burton and Miller (1971)]. However, the method presented in [Chandrasekhar and Rao (2004)] is applicable to rigid bodies only. In the present work, this method is extended to fluid bodies.

2 Mathematical Formulation

Consider an arbitrarily shaped three-dimensional, homogeneous, non-viscous, fluid body with density and acoustic velocity given by ρ_2 and c_2, re-
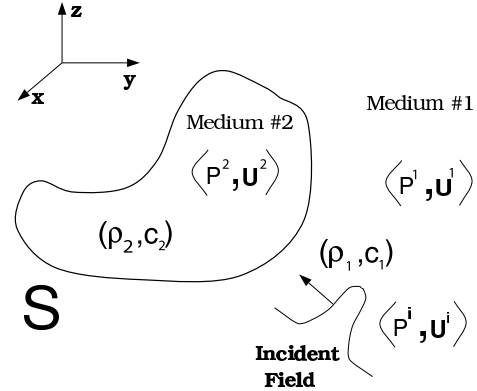

Figure 1: Arbitrary fluid body excited by an acoustic plane wave.

spectively. The body is placed in an infinite, homogeneous, non-viscous medium of density ρ_1 and velocity c_1 as shown in Fig. 1. A sound wave, propagating in medium 1, is incident on the obstacle.

Let (p_1, u_1) and (p_2, u_2) represent the total pressure and velocity fields in the media 1 and 2, respectively. In medium 1, p_1 and u_1 represent the sum of the incident, (p^i, u^i), and scattered pressure and velocity fields, (p^s, u^s), given by $p_1 = p^i + p^s$ and $u_1 = u^i + u^s$. In medium 2, p_2 and u_2 represent the fields penetrated into the obstacle. It is important to note that the incident fields are defined in the absence of the scatterer. It is customary to introduce a velocity potential Φ^i, $i = 1, 2$ such that $u^i = \nabla\Phi^i$ and $p^i = -j\omega\rho_i\Phi^i$, assuming harmonic time variation.

The acoustic scattering problem is solved by assuming two independent scalar source distributions σ_1 and σ_2. The source distributions σ_1 and σ_2 are slightly outside and inside of the surface S, respectively. The two source distributions completely describe the acoustic pressure and velocity fields both inside and outside the scatterer. Note that the outside fields p_1 and u_1 are generated by σ_1 and inside fields p_2 and u_2 are generated by σ_2, respectively. Using the potential theory and free space Green's function, the scattered velocity potential may be defined as

$$\Phi_i^s = \int_S \sigma_i(r') \, G_i(r,r') \, ds' \tag{1}$$

for the single layer formulation (SLF) case,

$$\Phi_i^s = \int_S \sigma_i(r') \frac{\partial G_i(r,r')}{\partial n'} \, ds' \tag{2}$$

for the double layer formulation (DLF) case, and

$$\Phi_i^s = \int_S \sigma_i(r') \left[j\alpha G_i(r,r') + j(1-\alpha)\frac{\partial G_i(r,r')}{\partial n'} \right] ds' \tag{3}$$

for the combined layer formulation (CLF) case, respectively. Note that, in Eq. (3), α is a combination constant typically chosen between 0 and 1. CLF reduces to the case of SLF when α is one and to the DLF when α is zero.

In Eqs. (1), (2), and (3)

$$G_i(r,r') = \frac{e^{-jk_i R}}{4\pi R}, \qquad i = 1,2 \tag{4}$$

and

$$R = \left| r - r' \right|, \tag{5}$$

r', r and $k_i = \omega/c_i$ represent the locations of the source point, location of the observation point, and the wave number in the i th medium, respectively. Both r and r' are defined with respect to a global coordinate origin $\bigcirc$. Also, note that in Eqs. (2) and (3), $\partial/\partial n'$ represents the normal derivative with respect to the source point r'.

The velocity potentials Φ_i^s, $i = 1$ and 2, are related to the pressure and velocity fields given by,

$$p_1 = -j\omega\rho_1 \left(\Phi_1^s + \Phi^i \right) \tag{6}$$

$$p_2 = -j\omega\rho_2 \Phi_2^s \tag{7}$$

$$u_1 = \nabla \left(\Phi_1^s + \Phi^i \right) \tag{8}$$

and

$$u_2 = \nabla \Phi_2^s. \tag{9}$$

The boundary conditions on the scatterer surface require the pressure and normal component of velocity fields to be continuous at the interface. By enforcing the continuity conditions of pressure and velocity fields at the surface S, the following set of coupled integral equations may be derived:

$$\rho_1 \left(\Phi_1^s + \Phi^i \right) = \rho_2 \Phi_2^s \tag{10}$$

and

$$\frac{\partial}{\partial n} \left(\Phi_1^s + \Phi^i \right) = \frac{\partial \Phi_2^s}{\partial n} \tag{11}$$

which implies

$$\rho_1 \Phi_1^s - \rho_2 \Phi_2^s = -\rho_1 \Phi^i \tag{12}$$

and

$$\frac{\partial \Phi_1^s}{\partial n} - \frac{\partial \Phi_2^s}{\partial n} = - \frac{\partial \Phi^i}{\partial n} \tag{13}$$

Substituting the Eqs. (1), (2) and (3) in Eqs. (12) and (13), we have

$$\rho_1 \int_S \sigma_1(r') \, G_1(r,r') \, ds' \\ - \rho_2 \int_S \sigma_2(r') \, G_2(r,r') \, ds' = -\rho_1 \Phi^i \tag{14}$$

$$\frac{\partial}{\partial n} \int_S \sigma_1(r') \, G_1(r,r') \, ds' \\ - \frac{\partial}{\partial n} \int_S \sigma_2(r') \, G_2(r,r') \, ds' = -\frac{\partial \Phi^i}{\partial n} \tag{15}$$

for the SLF case,

$$\rho_1 \int_S \sigma_1(r') \, \frac{\partial G_1(r,r')}{\partial n'} \, ds' \\ - \rho_2 \int_S \sigma_2(r')\frac{\partial G_2(r,r')}{\partial n'} \, ds' = -\rho_1 \Phi^i \tag{16}$$

$$\frac{\partial}{\partial n} \int_S \sigma_1(r')\frac{\partial G_1(r,r')}{\partial n'} \, ds' \\ - \frac{\partial}{\partial n} \int_S \sigma_2(r')\frac{\partial G_2(r,r')}{\partial n'} \, ds' = -\frac{\partial \Phi^i}{\partial n} \tag{17}$$

for the DLF case, and

$$j\alpha\,[\text{LHS of Eq. (14)}] \\ + j(1-\alpha)\,[\text{LHS of Eq. (16)}] = -\rho_1 \Phi^i \tag{18}$$

$$j\alpha \left[\text{LHS of Eq. (15)}\right]$$

$$+ j(1-\alpha)\left[\text{LHS of Eq. (17)}\right] = -\frac{\partial \Phi^i}{\partial n} \quad (19)$$

for the CLF case, respectively.

In the following, the mathematical steps are described, in detail, to obtain a numerical solution to SLF, DLF and CLF based on triangular patch modeling and MoM. The basic definitions regarding the patch model and the basis/testing functions required for MoM solution are same as described in [Chandrasekhar and Rao (2004)] and outlined here for the sake of completeness.

Assuming a suitable triangular patch model of the body, the basis function, defined over an edge connecting two triangles T_n^+ and T_n^-, is given by

$$f_n(r) = \begin{cases} 1, & r \in S_n, \\ 0, & \text{otherwise} \end{cases} \quad (20)$$

where S_n represents the region obtained by connecting the centroids of triangles $T_n^\pm$ to the nodes of edge n. Using these basis functions, the unknown source distribution σ_1 and σ_2 in Eqs. (14) - (19) may be approximated as

$$\sigma_i(r) = \sum_{n=1}^{N_e} x_{n,i} f_n(r) \quad (21)$$

for $i = 1$ and 2. In Eq. (21), $x_{n,i}$ represents the unknown coefficient to be determined.

3 Numerical Solution of SLF

In this section, the detailed derivation of the matrix equation generated in the solution of SLF is presented. Next, the equations for the far-field and near-fields are also derived.

3.1 *Derivation of Matrix Equations*

In this section, the integral equation, defined in Eqs. (14) and (15), is tranformed into a matrix equation using the MoM procedure presented in [Chandrasekhar and Rao (2004)].

Applying the testing procedure, Eq. (14) may be written as

$$\rho_1 < w_m, \int_S \sigma_1(r')\, G_1(r,r')\, ds' >$$

$$- \rho_2 < w_m, \int_S \sigma_2(r')\, G_2(r,r')\, ds' > \quad (22)$$

$$= -\rho_1 < w_m, \Phi^i > .$$

for $m = 1, 2, \cdots, N_e$. We observe that

$$< w_m, \int_S \sigma_i(r')\, G_i(r,r')\, ds' >$$

$$= \int_S \int_S \sigma_i(r')\, G_i(r,r')\, ds'ds$$

$$= \frac{A_m^+}{3} \int_S \sigma_i(r')\, G_i(r_m^{c+}, r')\, ds' \quad (23)$$

$$+ \frac{A_m^-}{3} \int_S \sigma_i(r')\, G_i(r_m^{c-}, r')\, ds'$$

where $A_m^\pm$ and $r_m^{c\pm}$ represents the area and the position vector to the centroid of $S_m^\pm$ connected to the mth-edge, respectively. Note that the surface integration over the testing functions in Eq. (23) is approximated by the integrand at the centroid of $S_m^\pm$ and multiplying by the area of the subdomain patch. This approximation is justified because the subdomains are sufficiently small which is a necessary requirement to obtain an accurate solution using the MoM. In a similar fashion, assuming the incident field to be a slowly varying function, the right hand side of Eq. (22) may be approximated as

$$< w_m, \Phi^i > = \int_S w_m(r)\, \Phi^i(r)\, ds$$

$$\approx \frac{A_m^+}{3}\Phi^i(r_m^{c+}) + \frac{A_m^-}{3}\Phi^i(r_m^{c-}). \quad (24)$$

Next, rewrite the Eq. (15), after extracting the principal value term, as

$$-\frac{\sigma_1}{2} + \fint_S \sigma_1(r')\, \frac{\partial G_1(r,r')}{\partial n}\, ds' - \frac{\sigma_2}{2}$$

$$- \fint_S \sigma_2(r')\, \frac{\partial G_2(r,r')}{\partial n}\, ds' = -\frac{\partial \Phi^i}{\partial n}, \quad (25)$$

where $\fint_S$ represents the integration over the surface excluding the principal value term *i.e.* $r = r'$. Here, note that the $\fint_S$ represents a well-behaved integral which can be evaluated using standard integration algorithms.

Then, the testing equation may be written as

$$- < w_m, \frac{\sigma_1}{2} >$$

$$+ < w_m, \int_S \sigma_1(r') \frac{\partial G_1(r,r')}{\partial n} ds' >$$

$$- < w_m, \frac{\sigma_2}{2} >$$

$$- < w_m, \int_S \sigma_2(r') \frac{\partial G_2(r,r')}{\partial n} ds' >$$

$$= - < w_m, \frac{\partial \Phi^i}{\partial n} > \tag{26}$$

for $m = 1, 2, \cdots, N_e$. Observe that

$$< w_m, \frac{\sigma_i}{2} > = \frac{1}{2} \left[\frac{A_m^+ \sigma_i(r_m^{c+}) + A_m^- \sigma_i(r_m^{c-})}{3} \right] \tag{27}$$

and,

$$< w_m, \int_S \sigma_i(r') \frac{\partial G_i(r,r')}{\partial n} ds' >$$

$$= \int_S \int_S \sigma_i(r') \frac{\partial G_i(r,r')}{\partial n} ds' ds$$

$$= \frac{A_m^+}{3} \int_S \sigma_i(r') \frac{\partial G_i(r_m^{c+},r')}{\partial n^+} ds' \tag{28}$$

$$+ \frac{A_m^-}{3} \int_S \sigma_i(r') \frac{\partial G_i(r_m^{c-},r')}{\partial n^-} ds'$$

Similarly, approximate the right hand side of Eq. (25) as

$$< w_m, \frac{\partial \Phi^i}{\partial n} > = \int_S w_m(r) \frac{\partial \Phi^i(r)}{\partial n} ds$$

$$\approx \frac{A_m^+}{3} \frac{\partial \Phi^i(r_m^{c+})}{\partial n} + \frac{A_m^-}{3} \frac{\partial \Phi^i(r_m^{c-})}{\partial n} \tag{29}$$

Thus, using Eqs. (23), (24), (27), (28), and (29), the testing equations may be written as

$$\rho_1 \left[\frac{A_m^+}{3} \int_S \sigma_1(r') G_1(r_m^{c+}, r') ds' \right.$$

$$+ \frac{A_m^-}{3} \int_S \sigma_1(r') G_1(r_m^{c-}, r') ds' \right]$$

$$- \rho_2 \left[\frac{A_m^+}{3} \int_S \sigma_2(r') G_2(r_m^{c+}, r') ds' \right. \tag{30}$$

$$+ \frac{A_m^-}{3} \int_S \sigma_2(r') G_2(r_m^{c-}, r') ds' \right]$$

$$= -\rho_1 \left[\frac{A_m^+}{3} \Phi^i(r_m^{c+}) + \frac{A_m^-}{3} \Phi^i(r_m^{c-}) \right]$$

and

$$- \frac{1}{2} \left[\frac{A_m^+ \sigma_1(r_m^{c+}) + A_m^- \sigma_1(r_m^{c-})}{3} \right]$$

$$+ \frac{A_m^+}{3} \int_S \sigma_1(r') \frac{\partial G_1(r_m^{c+},r')}{\partial n^+} ds'$$

$$+ \frac{A_m^-}{3} \int_S \sigma_1(r') \frac{\partial G_1(r_m^{c-},r')}{\partial n^-} ds'$$

$$- \frac{1}{2} \left[\frac{A_m^+ \sigma_2(r_m^{c+}) + A_m^- \sigma_2(r_m^{c-})}{3} \right] \tag{31}$$

$$- \frac{A_m^+}{3} \int_S \sigma_2(r') \frac{\partial G_2(r_m^{c+},r')}{\partial n^+} ds'$$

$$- \frac{A_m^-}{3} \int_S \sigma_2(r') \frac{\partial G_2(r_m^{c-},r')}{\partial n^-} ds'$$

$$= - \left[\frac{A_m^+}{3} \frac{\partial \Phi^i(r_m^{c+})}{\partial n} + \frac{A_m^-}{3} \frac{\partial \Phi^i(r_m^{c-})}{\partial n} \right]$$

for $m = 1, 2, \cdots, N_e$.

Substituting Eq. (21) into Eqs. (30) and (31), the matrix equation can be written as

$$Z_{slf} X = Y \tag{32}$$

where

$$Z_{slf} = \begin{bmatrix} Z^a & Z^b \\ Z^c & Z^d \end{bmatrix} \tag{33}$$

is a matrix of size $2N_e \times 2N_e$, and Z^a, Z^b, Z^c, and Z^d are submatrices of size $N_e \times N_e$. Further in Eq. (32), X and Y are column vectors of size $2N_e$ given by

$$X = \begin{bmatrix} x_{m,1} \\ x_{m,2} \end{bmatrix} \quad \text{and} \quad Y = \begin{bmatrix} y_{m,1} \\ y_{m,2} \end{bmatrix}. \tag{34}$$

for $m = 1, 2, \cdots, N_e$.

The matrix elements of Z^a, Z^b, Z^c, and Z^d are given by

$$z_{mn}^a = \rho_1 \left[P_{1,mn}^+ + P_{1,mn}^- \right] \tag{35}$$

$$z_{mn}^b = -\rho_2 \left[P_{2,mn}^+ + P_{2,mn}^- \right] \tag{36}$$

$$z_{mn}^c = \begin{cases} -\frac{A_m^+ + A_m^-}{6} + Q_{1,mn}^+ + Q_{1,mn}^- & \text{for } m = n \\ Q_{1,mn}^+ + Q_{1,mn}^- & \text{for } m \neq n \end{cases} \tag{37}$$

$$z_{mn}^d = \begin{cases} -\frac{A_m^+ + A_m^-}{6} - Q_{2,mn}^+ - Q_{2,mn}^- & \text{for } m = n \\ -Q_{2,mn}^+ - Q_{2,mn}^- & \text{for } m \neq n \end{cases} \tag{38}$$

where

$$P^{\pm}_{i,mn} = \frac{A^{\pm}_m}{3}\left[\int_{S^+_n} G_i(r^{c\pm}_m, r')\, ds' + \int_{S^-_n} G_i(r^{c\pm}_m, r')\, ds'\right] \tag{39}$$

$$Q^{\pm}_{i,mn} = \frac{A^{\pm}_m}{3}\left[\oint_{S^+_n}\frac{\partial G_i(r^{c\pm}_m, r')}{\partial n^{\pm}}ds' + \oint_{S^-_n}\frac{\partial G_i(r^{c\pm}_m, r')}{\partial n^{\pm}}ds'\right] \tag{40}$$

for $m = 1, 2, \cdots, N$ and $i = 1$ and 2. Integrals, appearing in Eqs. (39) and (40), are straight forward integrals over a triangular region. However, it is cautioned that the integrals have singular kernels and, for accurate solution, may be evaluated using the methods described in [Wilton, Rao, Glisson, Schaubert, Al-Bundak and Bulter (1984) and Hammer, Marlowe and Stroud (1956)].

The elements of the column vector Y are given by

$$y_{m,1} = -\rho_1\left[\frac{A^+_m}{3}\Phi^i(r^{c+}_m) + \frac{A^-_m}{3}\Phi^i(r^{c-}_m)\right]$$
$$y_{m,2} = -\frac{A^+_m}{3}\frac{\partial\Phi^i(r^{c+}_m)}{\partial n^+} - \frac{A^-_m}{3}\frac{\partial\Phi^i(r^{c-}_m)}{\partial n^-} \tag{41}$$

for $m = 1, 2, \cdots, N_e$.

Once the elements of the moment matrix Z and the forcing vector Y are determined, one may solve the resulting system of linear equations, Eq. (32), for the unknown column vector X.

3.2 Far-field Solution

Using simple algebra, for $r \to \infty$, Eq. (1) may be written as

$$\Phi^s = \frac{e^{-jk_1r}}{4\pi r}\int_S \sigma_1(r')\, e^{jk_1a_r\cdot r'}\, ds' \tag{42}$$

where a_r is the unit vector along the direction joining the cooridnate origin and the observation point. Next, utilizing Eq. (21), the far-scattered velocity potential may be written as

$$\begin{aligned}\Phi^s &= \frac{e^{-jk_1r}}{4\pi r}\int_S\sum_{n=1}^N x_{n,1} f_n(r')\, e^{jk_1a_r\cdot r'}\, ds' \\ &= \frac{e^{-jk_1r}}{4\pi r}\sum_{n=1}^N x_{n,1}\int_{S_n} e^{jk_1a_r\cdot r'}\, ds' \\ &= \frac{e^{-jk_1r}}{4\pi r}\sum_{n=1}^N x_{n,1}\left(\frac{A^+_n}{3}e^{jk_1a_r\cdot r^{c+}_n} + \frac{A^-_n}{3}e^{jk_1a_r\cdot r^{c-}_n}\right)\end{aligned} \tag{43}$$

Finally, scattering cross section S may be defined as

$$\begin{aligned}S &= 4\pi r^2\left|\frac{\Phi^s}{\Phi^i}\right|^2 \\ &= \frac{1}{4\pi}\left|\sum_{n=1}^N x_{n,1}\left(\frac{A^+_n}{3}e^{jk_1a_r\cdot r^{c+}_n} + \frac{A^-_n}{3}e^{jk_1a_r\cdot r^{c-}_n}\right)\right|^2\end{aligned} \tag{44}$$

assuming $|\Phi^i| = 1$.

3.3 Near-field Solution

Once the source distribution on the object is known, the scattered velocity potential at any point in space may be calculated using Eq. (1). Obviously, for the near-field calculation *i.e.* at any point whose farthest distance from the scatterer is small compared to wavelength, the integrals in Eq. (1) may be evaluated using the numerical procedures developed in [Wilton, Rao, Glisson, Schaubert, Al-Bundak and Bulter (1984) and Hammer, Marlowe and Stroud (1956)]. Note that, although the integrals involved are not singular the evaluation of these must be done carefully to obtain accurate results. Alternatively, the following simple numerical procedure may be employed to calculate the near-fields which is sufficient for many situations.

Let P denote the point of observation which may be outside or inside the scatterer. Let r_p represent the the position vector to P. Then, using Eq. (1),

we have

$$\Phi_i^s(r) = \int_S \sigma_i(r') \; G_i(r_p, r') \, ds'$$

$$\approx \sum_{n=1}^{N} x_{n,i} \left[\frac{G_i(r_p, r_n^{c+})A_n^+}{3} + \frac{G_i(r_p, r_n^{c-})A_n^-}{3} \right]$$

(45)

Note that since $x_{n,i}$, $i = 1$ and 2 is known, we can evaluate the expression Eq. (45) very easily.

4 Numerical Solution of DLF

In this section, a detailed derivation of the matrix equation generated in the solution of DLF along with the far-field and near-field calculations is presented.

4.1 Derivation of Matrix Equations

First of all, note that the LHS of the integral equation Eq. (16) is very similar to the LHS of Eq. (15) except some multiplication constants. Hence, the numerical processing of this equation follows similar steps as of Eq. (15). Thus, the final equation, after testing, leaving out the details, is given by

$$-\frac{\rho_1}{2} \left[\frac{A_m^+ \sigma_1(r_m^{c+}) + A_m^- \sigma_1(r_m^{c-})}{3} \right]$$

$$+ \frac{\rho_1 A_m^+}{3} \int_S \sigma_1(r') \frac{\partial G_1(r_m^{c+}, r')}{\partial n'^+} \, ds'$$

$$+ \frac{\rho_1 A_m^-}{3} \int_S \sigma_1(r') \frac{\partial G_1(r_m^{c-}, r')}{\partial n'^-} \, ds'$$

$$- \frac{\rho_2}{2} \left[\frac{A_m^+ \sigma_2(r_m^{c+}) + A_m^- \sigma_2(r_m^{c-})}{3} \right]$$

$$- \frac{\rho_2 A_m^+}{3} \int_S \sigma_2(r') \frac{\partial G_2(r_m^{c+}, r')}{\partial n'^+} \, ds'$$

$$- \frac{\rho_2 A_m^-}{3} \int_S \sigma_2(r') \frac{\partial G_2(r_m^{c-}, r')}{\partial n'^-} \, ds'$$

$$= -\rho_1 \left[\frac{A_m^+}{3} \Phi^i(r_m^{c+}) + \frac{A_m^-}{3} \Phi^i(r_m^{c-}) \right]$$

(46)

for $m = 1, 2, \cdots, N_e$.

Next, following the procedures developed in [Maue and Mitzner (1966)], Eq. (17) may be re-written as

$$\int_S a_n \bullet a_n' k_1^2 \sigma_1 G_1 ds'$$

$$+ \int_S \left(a_n' \times \nabla \sigma_1 \right) \bullet \left(a_n \times \nabla G_1 \right) ds'$$

$$- \int_S a_n \bullet a_n' k_2^2 \sigma_2 G_2 ds'$$

$$- \int_S \left(a_n' \times \nabla \sigma_2 \right) \bullet \left(a_n \times \nabla G_2 \right) ds'$$

$$= a_n \bullet \nabla \Phi^i$$

(47)

where a_n and a_n' represent the unit normal vectors at r and r', respectively.

Testing the Eq. (47) with the testing functions defined in Eq. (20), we have

$$< w_m, \int_S a_n \bullet a_n' k_1^2 \sigma_1 G_1 \, ds' >$$

$$+ < w_m, \int_S (a_n' \times \nabla \sigma_1) \bullet (a_n \times \nabla G_1) \, ds' >$$

$$- < w_m, \int_S a_n \bullet a_n' k_2^2 \sigma_2 G_2 \, ds' >$$

$$- < w_m, \int_S (a_n' \times \nabla \sigma_2) \bullet (a_n \times \nabla G_2) \, ds' >$$

$$= < w_m, a_n \bullet \nabla \Phi^i >$$

(48)

for $m = 1, 2, \cdots, N_e$. By using similar approximation as for Eq. (23), the first and the third terms of Eq. (48) may be re-written as

$$< w_m, \int_S a_n \bullet a_n' k_i^2 \sigma_i G_i ds' >$$

$$= \int_S w_m(r) \int_S a_n \bullet a_n' k_i^2 \sigma_i(r') G_i(r,r') \, ds' ds$$

$$\approx \frac{A_m^+}{3} a_m^+ \bullet \int_S a_n' k_i^2 \sigma_i(r') G_i(r_m^{c+}, r') \, ds'$$

$$+ \frac{A_m^-}{3} a_m^- \bullet \int_S a_n' k_i^2 \sigma_i(r') G_i(r_m^{c-}, r') \, ds'$$

(49)

Next, consider the evaluation of second and fourth terms of Eq. (48). Following the numerical procedure developed in [Chandrasekhar and Rao (2004)], we have

$$< w_m, \int_S (a_n' \times \nabla \sigma_i) \bullet (a_n \times \nabla G_i) \, ds' >$$

$$= \ell_m \bullet \left[A_i(r_m^{cp-}) - A_i(r_m^{cp+}) \right]$$

(50)

where ℓ_m is the vector along the edge m and

$$A = \int_S a_n \times \nabla \sigma \, G \, ds' \tag{51}$$

Again, note that the RHS of Eq. (48) is the same as in the case of SLF, given by Eq. (31).

Thus, using Eqs. (49) and (50), Eqs. (48) may be re-written as

$$
\begin{aligned}
&\frac{A_m^+}{3} a_m^+ \bullet \int_S a_n' k_1^2 \sigma_1(r') G_1(r_m^{c+}, r') \, ds' \\
&+ \frac{A_m^-}{3} a_m^- \bullet \int_S a_n' k_1^2 \sigma_1(r') G_1(r_m^{c-}, r') \, ds' \\
&+ \ell_m \bullet \left[A_1(r_m^{cp-}) - A_1(r_m^{cp+}) \right] \\
&- \frac{A_m^+}{3} a_m^+ \bullet \int_S a_n' k_2^2 \sigma_2(r') G_2(r_m^{c+}, r') \, ds' \\
&- \frac{A_m^-}{3} a_m^- \bullet \int_S a_n' k_2^2 \sigma_2(r') G_2(r_m^{c-}, r') \, ds' \\
&- \ell_m \bullet \left[A_2(r_m^{cp-}) - A_2(r_m^{cp+}) \right] \\
&= -\left[\frac{A_m^+}{3} \frac{\partial \Phi^i(r_m^{c+})}{\partial n} + \frac{A_m^-}{3} \frac{\partial \Phi^i(r_m^{c-})}{\partial n} \right]
\end{aligned} \tag{52}
$$

for $m = 1, 2, \cdots, N_e$.

Substituting Eq. (21) into Eqs. (46) and (52), the matrix equation can be written as

$$Z_{dlf} X = Y \tag{53}$$

where

$$Z_{dlf} = \begin{bmatrix} Z^a & Z^b \\ Z^c & Z^d \end{bmatrix} \tag{54}$$

is a matrix of size $2N_e \times 2N_e$, and Z^a, Z^b, Z^c, and Z^d are submatrices of size $N_e \times N_e$. Further in Eq. (54), X and Y are coloumn vectors of size $2N_e$ given by

$$X = \begin{bmatrix} x_{m,1} \\ x_{m,2} \end{bmatrix} \quad \text{and} \quad Y = \begin{bmatrix} y_{m,1} \\ y_{m,2} \end{bmatrix}. \tag{55}$$

for $m = 1, 2, \cdots, N_e$.

The matrix elements of Z^a, Z^b, Z^c, and Z^d are

given by

$$z_{mn}^a = \begin{cases} \rho_1 \left[\frac{A_m^+ + A_m^-}{6} + Q_{1,mn}^+ + Q_{1,mn}^- \right] & \text{for } m = n \\ \rho_1 \left[Q_{1,mn}^+ + Q_{1,mn}^- \right] & \text{for } m \neq n \end{cases} \tag{56}$$

$$z_{mn}^b = \begin{cases} \rho_2 \left[\frac{A_m^+ + A_m^-}{6} - Q_{2,mn}^+ - Q_{2,mn}^- \right] & \text{for } m = n \\ -\rho_2 \left[Q_{2,mn}^+ + Q_{2,mn}^- \right] & \text{for } m \neq n \end{cases} \tag{57}$$

$$z_{mn}^c = P_{1,mn}^+ + P_{1,mn}^- + \ell_m \bullet \left[A_{1,mn}^+ - A_{1,mn}^- \right] \tag{58}$$

$$z_{mn}^d = -P_{2,mn}^+ - P_{2,mn}^- - \ell_m \bullet \left[A_{2,mn}^+ - A_{2,mn}^- \right] \tag{59}$$

$$P_{i,mn}^{\pm} = \frac{k_i^2 A_m^{\pm}}{3} a_m^{\pm} \bullet \left[\int_{S_n^+} a_n' \, G_i(r_m^{c\pm}, r') \, ds' \right. \\ \left. + \int_{S_n^-} a_n' \, G_i(r_m^{c\pm}, r') \, ds' \right] \tag{60}$$

$$Q_{i,mn}^{\pm} = \frac{A_m^{\pm}}{3} \left[\int_{S_n^+} \frac{\partial G_i(r_m^{c\pm}, r')}{\partial n'^+} ds' \right. \\ \left. + \int_{S_n^-} \frac{\partial G_i(r_m^{c\pm}, r')}{\partial n'^-} ds' \right] \tag{61}$$

$$A_{i,mn}^{\pm} = \ell_n \left[\frac{1}{A_n^+} \int_{T_n^+} G_i(r_m^{cp\pm}, r') ds' \right. \\ \left. + \frac{1}{A_n^-} \int_{T_n^-} G_i(r_m^{cp\pm}, r') ds' \right] \tag{62}$$

for $m = 1, 2, \cdots, N$ and $i = 1$ and 2. Further, the elements of the column vector Y are same as in the case of SLF and given by Eq. (41).

The integrals, appearing in Eqs. (60) - (62), are straight forward integrals over a triangular region. However, it is cautioned that the integrals have singular kernels and, for accurate solution, may be evaluated using the methods described in [Wilton, Rao, Glisson, Schaubert, Al-Bundak and Bulter (1984) and Hammer, Marlowe and Stroud (1956)].Once the elements of the moment matrix Z and the forcing vector Y are determined, one may solve the resulting system of linear equations, Eq. (32), for the unknown column vector X.

4.2   Far-field Solution

The numerical evaluation of the far-fields for this case follow the similar steps as in the SLF case.

Thus,

$$\frac{\partial G_1(r,r')}{\partial n'} = \frac{1 + jk_1 R}{R^2} \frac{e^{-jk_1 R}}{4\pi R} \left[a'_n \cdot (r - r')\right]$$
$$\approx \frac{e^{-jk_1 r}}{4\pi r} e^{jk_1 a_r \cdot r'} \left(jk_1 a'_n \cdot r'\right) \tag{63}$$

Next, for a far-field observation point, using Eq. (63), Eq. (2) may be written as

$$\Phi^s = \frac{e^{-jk_1 r}}{4\pi r} \int_S \sigma_1(r') \, jk_1 \, (a'_n \cdot r') \, e^{jk_1 a_r \cdot r'} \, ds' \tag{64}$$

Utilizing Eq. (21), the far-scattered velocity potential may be written as

$$\Phi^s = \frac{e^{-jk_1 r}}{4\pi r} \int_S \sum_{n=1}^N x_{1,n} f_n(r') jk_1 (a'_n \cdot r') e^{jk_1 a_r \cdot r'} ds'$$
$$= \frac{e^{-jk_1 r}}{4\pi r} \sum_{n=1}^N x_{1,n} \int_{S_n} jk_1 (a'_n \cdot r') e^{jk_1 a_r \cdot r'} ds'$$
$$= \frac{jk_1 e^{-jk_1 r}}{4\pi r} \sum_{n=1}^N \frac{x_{1,n}}{3} \left(A_n^+ a_n^+ \cdot r_n^{c+} e^{jk_1 a_r \cdot r_n^{c+}}\right.$$
$$\left. + A_n^- a_n^- \cdot r_n^{c-} e^{jk_1 a_r \cdot r_n^{c-}}\right) \tag{65}$$

Finally, scattering cross section S is given by

$$S = 4\pi r^2 \left|\frac{\Phi^s}{\Phi^i}\right|^2$$
$$= \frac{k_1^2}{4\pi} \left|\sum_{n=1}^N \frac{x_{1,n}}{3} \left(A_n^+ a_n^+ \cdot r_n^{c+} e^{jk_1 a_r \cdot r_n^{c+}}\right.\right. \tag{66}$$
$$\left.\left. + A_n^- a_n^- \cdot r_n^{c-} e^{jk_1 a_r \cdot r_n^{c-}}\right)\right|^2$$

assuming $|\Phi^i| = 1$.

4.3 Near-field Solution

Let P denote the point of observation and let r_p represent the position vector to P. Then, using Eq. (2),

$$\Phi_i^s(r) = \int_S \sigma_i(r') \frac{\partial G_i(r_p, r')}{\partial n'} ds'$$
$$\approx \sum_{n=1}^N x_{1,n} \frac{1}{3} \left\{ \frac{\partial G_i(r_p, r_n^{c+})}{\partial n^+} A_n^+ + \frac{\partial G_i(r_p, r_n^{c-})}{\partial n^-} A_n^- \right\} \tag{67}$$

Note that, the normal derivatives, $\frac{\partial G_i(r_p, r_n^{c\pm})}{\partial n^\pm}$ in Eq. (67) may be analytically evaluated. Thus, since $x_{1,n}$ are available from the matrix solution, one can calculate the near scattered fields in an easy manner.

5 Numerical Solution of CLF

In this section, the numerical solution of the CLF, presented in Eq. (16) and Eq. (17), is developed. Note that the CLF is basically a linear combination of the SLF and the DLF presented in sections III and IV, respectively. Thus, the moment solution to the CLF is as follows:

Derivation of Matrix Equations

Using the numerical procedures developed in Sections III and IV, the matrix equation for the CLF case may be given as

$$Z_{clf} X = Y \tag{68}$$

where Z is an $2N_e \times 2N_e$ matrix and X and Y are column vectors of length $2N_e$. Elements of Z-matrix are given by

$$Z_{clf} = j\alpha Z_{slf} + j(1-\alpha) Z_{dlf} \tag{69}$$

Lastly, note that the elements of Y-matrix are same as that of the SLF and the DLF cases and given by Eq. (41).

Far-field Solution

For far-field observation point, Eq. (3) may be written as

$$\Phi^s = \frac{e^{-jk_1r}}{4\pi r}\int_S \sigma_1(r')\left\{j\alpha+j(1-\alpha)\left[jk_1 a_n' \cdot r'\right]\right\}$$

$$e^{jk_1 a_r \cdot r'}ds'$$

$$= \frac{e^{-jk_1r}}{4\pi r}\int_S \sigma_1(r')\left\{j\alpha-(1-\alpha)\left[k_1 a_n' \cdot r'\right]\right\}$$

$$e^{jk_1 a_r \cdot r'}ds'$$

(70)

Next, utilizing Eq. (70), the far-scattered velocity potential may be written as

$$\Phi^s$$

$$= \frac{e^{-jk_1r}}{4\pi r}\int_S \sum_{n=1}^N x_{1,n} f_n(r')\left\{j\alpha-k_1(1-\alpha)(a_n' \cdot r')\right\}$$

$$e^{jk_1 a_r \cdot r'}ds'$$

$$= \frac{e^{-jk_1r}}{4\pi r}\sum_{n=1}^N x_{1,n}\int_{S_n}\left\{j\alpha-k_1(1-\alpha)(a_n' \cdot r')\right\}$$

$$e^{jk_1 a_r \cdot r'}ds'$$

$$= \frac{e^{-jk_1r}}{4\pi r}\sum_{n=1}^N \frac{x_{1,n}}{3}\left[j\alpha\left(A_n^+ e^{jk_1 a_r \cdot r_n^{c+}}+A_n^- e^{jk_1 a_r \cdot r_n^{c-}}\right)\right.$$

$$-k_1(1-\alpha)$$

$$\left.\left(A_n^+ a_n^+ \cdot r_n^{c+} e^{jk_1 a_r \cdot r_n^{c+}}+A_n^- a_n^- \cdot r_n^{c-} e^{jk_1 a_r \cdot r_n^{c-}}\right)\right]$$

(71)

Finally, scattering cross section S is given by

$$S = 4\pi r^2 \left|\frac{\Phi^s}{\Phi^i}\right|^2$$

$$= \frac{1}{4\pi}\left|\sum_{n=1}^N \frac{x_{1,n}}{3}\left[j\alpha\left(A_n^+ e^{jk_1 a_r \cdot r_n^{c+}}+A_n^- e^{jk_1 a_r \cdot r_n^{c-}}\right)\right.\right.$$

$$-k_1(1-\alpha)\left(A_n^+ a_n^+ \cdot r_n^{c+} e^{jk_1 a_r \cdot r_n^{c+}}\right)$$

$$\left.\left.-k_1(1-\alpha)\left(A_n^- a_n^- \cdot r_n^{c-} e^{jk_1 a_r \cdot r_n^{c-}}\right)\right]\right|^2$$

(72)

assuming $|\Phi^i| = 1$.

Near-field Solution

Let P denote the point of observation and let r represent the the position vector to P. Then, using Eq. (3),

$$\Phi_i^s(r)$$

$$= \int_S \sigma_i(r')\left\{j\alpha G_i(r_p,r')+j(1-\alpha)\frac{\partial G_i(r_p,r')}{\partial n'}\right\}ds'$$

$$\approx \sum_{n=1}^N \frac{x_{i,n}}{3}\left\{G_i(r_p,r_n^{c+})A_n^+ + G_i(r_p,r_n^{c-})A_n^-\right\}$$

$$+j(1-\alpha)$$

$$\frac{x_{i,n}}{3}\left\{\frac{\partial G_i(r_p,r_n^{c+})}{\partial n^+}A_n^+ + \frac{\partial G_i(r_p,r_n^{c-})}{\partial n^-}A_n^-\right\}$$

(73)

5.1 Incident Field Equation

For the plane wave incidence,

$$\Phi^i = e^{jkk \cdot r}$$

(74)

where the propagation vector k is

$$k = \sin\theta_o \cos\phi_0 a_x + \sin\theta_o \sin\phi_0 a_y + \cos\theta_o a_z$$

(75)

and (θ_0, ϕ_0) defines the angle of arrival of the plane wave in terms of the usual spherical coordinate convention.

6 Numerical Results

In this section, several numerical results for the edge-based solution of SLF, DLF and CLF for fluid bodies, discussed so far in this work, is presented. The CLF numerical results are based on BM approach and the α is taken as $j0.1$ The examples considered are: a) a sphere, b) a cube and c) a marine body such as a fish. For all cases, the body is placed at the center of the coordinate system and the plane wave is traveling along the $-Z$-axis. For spherical geometry, the numerical

results are validated by comparing with the exact solution [Bowman, Senior and Uslenghi (1969)].

As a first example, consider a air bubble of radius 1m suspended in water. For numerical purposes, the spherical air bubble is modeled by 308 triangular patches and 462 edges resulting in a 924×924 matrix. The modeling is done by first dividing the θ and ϕ directions into 12 and 14 equal segments each, respectively. This results in triangular patches at the sphere caps and quadrilateral patches in between. By joining the diagonal of the quadrilateral patch, the triangular discretization may be obtained. The density of air in the bubble is 1.3 kg/m^3 and the velocity of sound as 331.45 m/s. Similarly, density of water is 1000 kg/m^3 and the velocity of sound as 1510.6 m/s. Fig. 2 shows the scattering cross section S as a function of the polar angle θ for spherical air bubble suspended in water for the case of $k = 1\ m^{-1}$. It is evident from the figures that the edge-based methods compare very well with the exact solution.

As a next example, consider a Carbon Tetrachloride (CCl_4) spherical inclusion of radius 1 m suspended in water. The spherical inclusion is modeled in the same way as in the previous example. The density of spherical inclusion is 1594 kg/m^3 and the velocity of sound as 930 m/s. Similarly, the density of water is 1000 kg/m^3 and the velocity of sound as 1510.6 m/s. Fig. 3 shows the scattering cross section S as a function of the polar angle θ for spherical air bubble suspended in water for the case of $k = 1\ m^{-1}$. Again, a good comparison is noted with the exact solution.

Next, consider the case of a cube filled with water with side length l= 1.0 m suspended in air. The case of a cube presents a challenging task of handling sharp edges and corners. To obtain a triangular patch model, each side of the cube is divided into 4 equal segments resulting in 96 square patches on the cube. By joining the diagonals, one gets 192 triangular patches and 288 edges resulting in a 576×576 matrix. Fig. 4 show the scattering cross section S as a function of θ in the yz-plane. For comparison, the patch-based MoM solution [Rao Raju and Sun (1992)] is also presented. It is evident from the figures that both re-
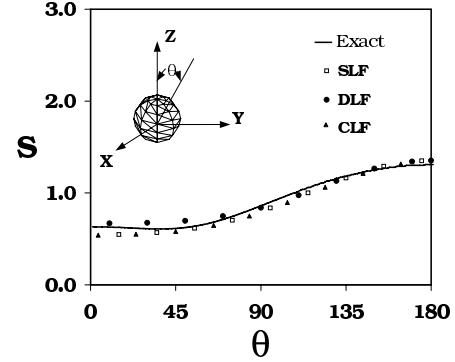

Figure 2: Scattering cross section versus polar angle for a plane wave incident on a spherical air bubble ($k_1 a = 1, \rho_2 = 1.3\ kg/m^3, c_2 = 331.45\ m/s$) suspended in water ($\rho_1 = 1000\ kg/m^3, c_1 = 1510.6\ m/s$).
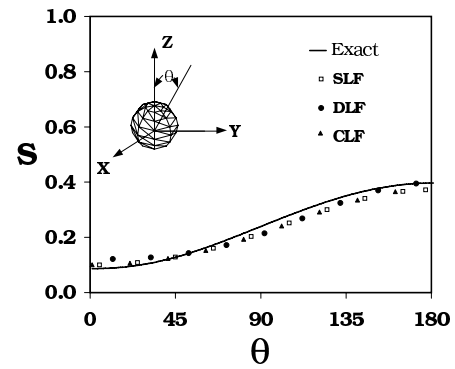

Figure 3: Scattering cross section versus polar angle for a plane wave incident on a spherical inclusion CCL_4 ($k_1 a = 1, \rho_2 = 1594\ kg/m^3, c_2 = 930\ m/s$) suspended in water ($\rho_1 = 1000\ kg/m^3, c_1 = 1510.6\ m/s$).
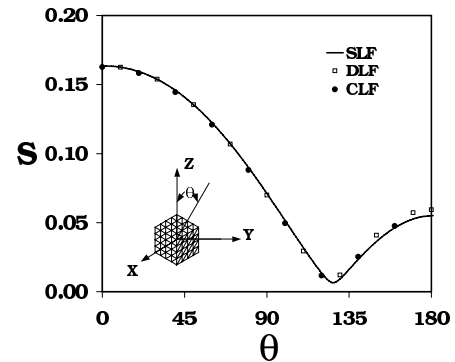

Figure 4: Scattering cross section versus polar angle for a plane wave incident on a water-filled cube ($k_1 \ell = 1, \rho_2 = 1000\ kg/m^3, c_2 = 1510.6\ m/s$) suspended in air ($\rho_1 = 1.3\ kg/m^3, c_1 = 331.45\ m/s$).

sults compare very well with each other.

As a last example, consider an highly arbitrarily-shaped, complex body, a dolphin as shown in Fig. 5, located in water. Note that the dolphin is not a fluid body in reality. However, we treat this case as a fluid body to show the ease of modeling and solving such complex problems with the present method. Although there is no comparison to make, this example to illustrates the applicability of present method to highly complex objects such as marine life. The maximum dimensions of the dolphin in length, width, and thickness are 1.5 m , 0.4 m, and 0.4 m, respectively. The marine object is modeled by 1646 triangular patches resulting in 2469 edges. Hence, in this solution scheme, the matrix dimension is 4938. The dolphin is placed in the coordinate system such that the center line along the body is at $45°$ elevation angle. The body excited by the plane wave given by Eq. (75). Figs. 6 and 7 show the scattering cross section in the elevation plane and azimuthal plane, respectively. Observe that the scattering cross section is low since for the material values chosen, the reflection coefficient of the dolphin is of the order of 0.1.
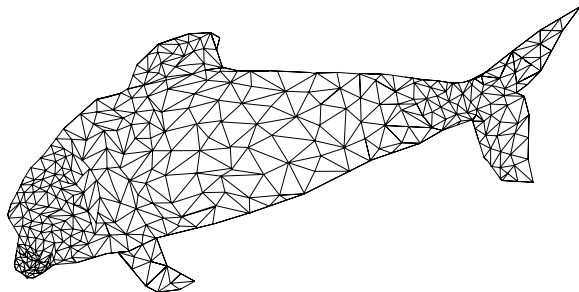

Figure 5: Trinagulated model of a dolphin.

Finally, in Fig. 8, the inverse condition number vs frequency for an air bubble of the first example for three different formulations is presented. Notice that both the SLF and the DLF exhibit instability problems at respective characteristic frequencies. However, the CLF is free from these problems. Although not reported, a similar trend for other geometries also noted.
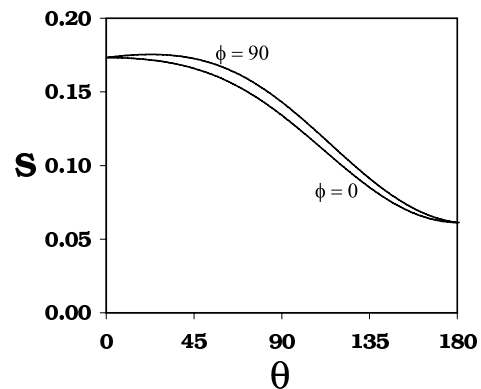

Figure 6: Scattering cross section versus polar angle for a plane wave incident on a dolphin ($\rho_2 = 1100\,kg/m^3, c_2 = 1700\,m/s$) in water ($\rho_1 = 1000\,kg/m^3, c_1 = 1510.6\,m/s$).
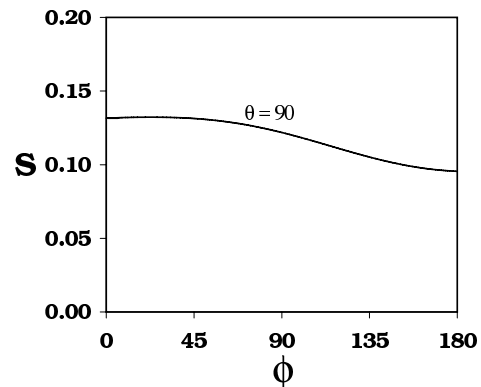

Figure 7: Scattering cross section versus polar angle for a plane wave incident on a dolphin ($\rho_2 = 1100\,kg/m^3, c_2 = 1700\,m/s$) in water ($\rho_1 = 1000\,kg/m^3, c_1 = 1510.6\,m/s$).
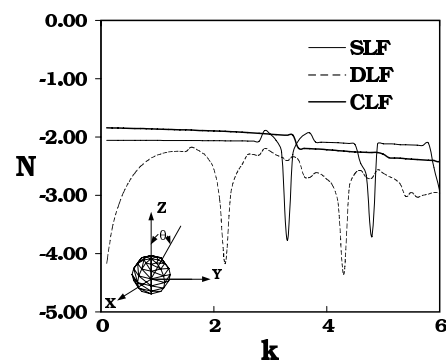

Figure 8: Inverse condition number vs. frequency for a spherical air bubble ($k_1 a = 1, \rho_2 = 1.3\,kg/m^3, c_2 = 331.45\,m/s$) suspended in water ($\rho_1 = 1000\,kg/m^3, c_1 = 1510.6\,m/s$).

7   Conclusions

In this work, a numerical solution, based on the method of moments, is presented to the acoustic scattering problem by arbitrarily-shaped, three-dimensional, fluid bodies. The governing integral equations are derived using the source distribution concept and the potential theory. Three different formulations *viz.* SLF, DLF and CLF methods are presented. Note that the CLF method is valid at all frequencies free from the so-called internal resonance problem. Further, the methodology is simple, efficient and applicable to a large class of problems.

References

Amini, S.; Wilton, D. T. (1986): An investigation of Boundary element methods for the exterior acoustic problem, *Computational Methods in Applied Mechanical Engineering*, vol 54, pp 49-65.

Benthien, W.; Schenck, H. A. (1997): Nonexistence and Nonuniqueness problems associated with integral equation methods in acoustics, *Computers & Structures*, vol 65, pp 295-305.

Bowman, J. J.; Senior, T. B. A.; Uslenghi, P. L. E. (1969): *Electromagnetic and Acoustic Scattering by Simple Shapes*, North Holland Publishing Company, Amsterdam.

Brakhage, H.; Werner, P. (1965): U ber das Dirichletsche Aussenraumproblem fur die Helmholtzsche Schwingungsgleichung, *Arch. Math.*, vol 16, pp 325-329.

Burton, A. J.; Miller, G. F. (1971): The application of integral equation methods to the numerical solution of some exterior boundary value problems. *Proceedings of Royal Society, London*, vol A323, pp 601-618.

Callsen, S.; von Estorff, O.; Zaleski, O.(2004): Direct and Indirect Approach of a Desingularized Boundary Element Formulation for Acoustical Problems. *CMES: Computer Modeling in Engineering & Sciences*, vol 6, no 5, pp 421-430.

Chandrasekhar, B; Rao, S. M. (2004): Elimination of internal resonance problem associated with acoustic scattering by three dimensional rigid body, *Journal of Acoustical Society of America*, vol 115, No 6, pp 2731-2737.

Chen, I. L. (2006): Using the Method of Fundamental Solutions in Conjunction with the Degenerate Kernel in Cylindrical Acoustic Problems, *J. Chinese Institute of Engineers*, vol 29, no 3, pp 445-457.

Chen, J. T.; Chen, I. L.; Chen, K. H. (2006): A unified formulation for the spurious and fictitious frequencies in acoustics using the singular value decomposition and Fredholm alternative theorem, *J. Comp. Acoustics*, vol 14, no 2, pp 157-183.

Chien, C. C.; Raliyah, H.; Alturi, S. N. (1990): An effective method for solving the hyper singular integral equations in 3-D acoustics. *Journal of Acoustical Society of America*, **88**, 918-937 (1990).

Hammer, P. C.; Marlowe, O. P.; Stroud, A. H. (1956): Numerical integration over simplxes and cones, *Math. Tables Aids Comp*, vol 10, pp 130-138.

Harrington, R. F.(1968): *Field computation by Method of Moments*, MacMillan, New York.

Kellog, O. D. (1929): *Foundations of Potential Theory*, F. Ungar Publishing, New York, (Also in Dover Reprint).

Leis. R. (1965): Zur Dirichletschen Randwertaufgabe des Auenraumes der Schwingungsgleichung, *Math. Z*, vol 90, pp 205-211.

Meyer, W. L.; Bell, W. A.; Zinn, B. T.; Stallybras, M. P. (1978): Boundary integral solutions of three dimensional acoustic radiation problems. *Journal of Sound and Vibration*, vol 59, pp 245-262.

Maue, A. W. (1949): Zur Formulierung eines allgemeinen Beugungsproblems durch eine Integralgleichung, *Journal of Physics*, vol 126, pp 601-618.

Mitzner, K. M. (1966): Acoustic scattering from an interface between media of greatly different density. *Journal of Mathematical Physics*, vol 7, pp 2053-2060.

Panich, O. I. (1965): On the question of the solvability of the exterior boundary problemfor wave equation and Maxwell's equation (in Russian), *Usp. Mat. Nauk*, vol 20, pp 221-226.

Qian, Z. Y.; Han, Z. D.; Atluri, S. N. (2004): Directly Derived Non-Hyper-Singular Boundary Integral Equations for Acoustic Problems, and Their Solution through Petrov-Galerkin Schemes, *CMES: Computer Modeling in Engineering & Sciences*, vol 5, no 6, pp 541-562.

Qian, Z. Y.; Han, Z. D.; Ufimtsev, P; Atluri, S. N. (2004): Non-Hyper-Singular Boundary Integral Equations for Acoustic Problems, Implemented by the Collocation-Based Boundary Element Method, *CMES: Computer Modeling in Engineering & Sciences*, vol 6, no 2, pp 133-144.

Rao, S. M.; Raju, P. K.; Sun, S. P. (1991): Application of Method of Moments to Acoustic Scattering From Multiple Infinitely Long Fluid Filled Cylinders, *Computers and Structures*, vol 39, pp 129-134.

Rao, S. M.; Raju, P. K; Sun, S. P. (1992): Application of the method of moments to acoustic scattering from fluid filled bodies of arbitrary shape, *Communications in Applied Numerical Methods*, vol 8, pp 117-128.

Schenck, H.A. (1968): Improved integral formulation for acoustic radiation problems, *Journal of Acoustical Society of America*, vol 44, pp 41-58.

Seybert. A. F.; Casey, D. K. (1988): An inegral equation method for copuled fluid/fluid scattering in three dimensions, *Journal of Acoustical Society of America*, vol 84, pp 379-384.

Sun, S. P. (1991): Application of Method of Moments to Acoustic Scattering, *Ph.D. Thesis, Auburn University*.

Wilton, D. R.; Rao, S. M.; Glisson, A. W.; Schaubert, D. H.; Al-Bundak, O. M.; Bulter, C. M. (1984): Potential Integrals for uniform and linear source distributions on polygons and polyhedra domains, *IEEE transactions, Antennas Propagation*, vol AP-32, pp 276-281.

Tobocman, W. (1984a): Calculation of acoustic wave scattering by means of the Helmholtz integral equation I, *Journal of Acoustical Society of America*, vol 76, pp 595-607.

Tobocman, W. (1984b): Calculation of acoustic wave scattering by means of the Helmholtz integral equation II, *Journal of Acoustical Society of America*, vol 76, pp 1549-1554.

Yan, Z. Y.; Cui, F. S.; Hung, K. C. (2005): Investigation on the Normal Derivative Equation of Helmholtz Integral Equation in Acoustics. *CMES: Computer Modeling in Engineering & Sciences*, vol 7, no 1, pp 97-106.